გ

#### Research Article

Nader A. A. Edress\*, Saudy Darwish, and Amir Ismail

# Geochemical characterization of the source rock intervals, Beni-Suef Basin, West Nile Valley, Egypt

https://doi.org/10.1515/geo-2020-0306 received May 17, 2021; accepted October 09, 2021

Abstract: Geochemical and lithological investigations in the WON C-3X well record five organic-matter-rich intervals (OMRIs) of effective source rocks. These OMRIs correspond to moderate and good potentials. Two of these intervals occurred within the L-Kharita member of the Albian age represent 60.97% of the entire Albian thickness. The rest of OMRIs belongs to the Abu-Roash G and F members of the Late Cenomanian-Santonian age comprising 17.52 and 78.66% of their total thickness, respectively. The calculated heat flow of the studied basin is high within the range of 90.1–95.55 mW/m<sup>2</sup> from shallower Abu-Roash F to deeper L-Kharita members. This high-heat flow is efficient for shallowing in the maximum threshold expulsion depth in the studied well to 2,000 m and active source rock depth limit to 2,750 m. Thermal maturity and burial history show that the source rock of L-Kharita entered the oil generation from 97 Ma till the late oil stage of 7.5 Ma, whereas the younger Abu-Roash G and F members have entered oil generation since 56 Ma and not reached peak oil yet. Hence, the source rock intervals from Abu-Roash F and G are promising for adequate oil generation.

**Keywords:** source rocks, Abu-Roash F-G, L-Kharita, OMrich interval, expulsion threshold depth, ASDL, heat flow, burial history

ORCID: Nader A. A. Edress 0000-0002-7320-486X; Amir Ismail 0000-0003-1167-0483

AIIII ISIIIdil 0000-0005-1107-0465

#### 1 Introduction

The Beni Suef Basin (BSB) is located almost 150 km south of Cairo, Egypt. The basin is separated into two provinces: the Western (WON) and the Eastern (EOP) provinces. It lies between longitudes 31° 30′ and 29° 50′ E and latitudes 29° 25′ and 28° 31′ N [1,2]. This basin is considered as a part of the North West (NW) rift system in the northeast African plate that was initiated at Early Cretaceous (Figure 1a). The BSB is a rift basin, which has been evaluated for petroleum exploration throughout the last two decades and is stationarily considered a promising region presently for the future hydrocarbon productivity [3,4].

The WON-C area, which is the study area, covers about  $42 \, \mathrm{km^2}$ , situated west of the Nile at the northern part of the Western Desert, bounded by latitudes 27° 00′ 00″ and 29° 17′ 00″ N and longitudes 30° 30′ 00″ and 32° 00′ 00″ E, with elevation ranging between  $\cong \pm 27 \, \mathrm{m}$  from the mean sea level, which represents the development lease of WON-C (Figure 2b).

The study area is under exploration so far and considered as one of the main prospective portions for petroleum exploration to the west of the Nile river. It was discovered in January 2011 through the drilling of WON-C-1X, which had been drilled to a total depth of 3741.42 m with 30.48 m drilled in the basement. A sandstone body of  $\cong$  (6.09–9.01 m) net sandstone of Abu-Roash G member is producing oil at a rate of 298 barrels of oil per day (BOPD). Moreover, the production of crude oil in the well is characterized by low American Petroleum Institute (API) gravity (25 API) and low pour point (-3°C [26.6°F]). From more than 30 exploratory and development wells scattered across the examined area, 4 were selected for the structural evaluation and attribute result integration of the study area. These wells are WON-C-1X, WON-C-2X, WON-C-3X, and WON-C-18 (Figure 1b).

The BSB has been explored in 1997. The oil field of the BSB was discovered by the Seagull Energy Corporation, and five more oil fields were discovered by Qarun Petroleum

<sup>\*</sup> Corresponding author: Nader A. A. Edress, Geology Department, Faculty of Sciences, Helwan University, Cairo, Egypt, e-mail: nedress@outlook.com, nedress@science.helwan.edu.eg
Saudy Darwish: Exploration Department, Agiba Petroleum
Company, Nasr City, Cairo, Egypt, e-mail: saudy.darwish@agiba.com
Amir Ismail: Geology Department, Faculty of Sciences, Helwan University, Cairo, Egypt, e-mail: amir\_ismail@science.helwan.edu.eg

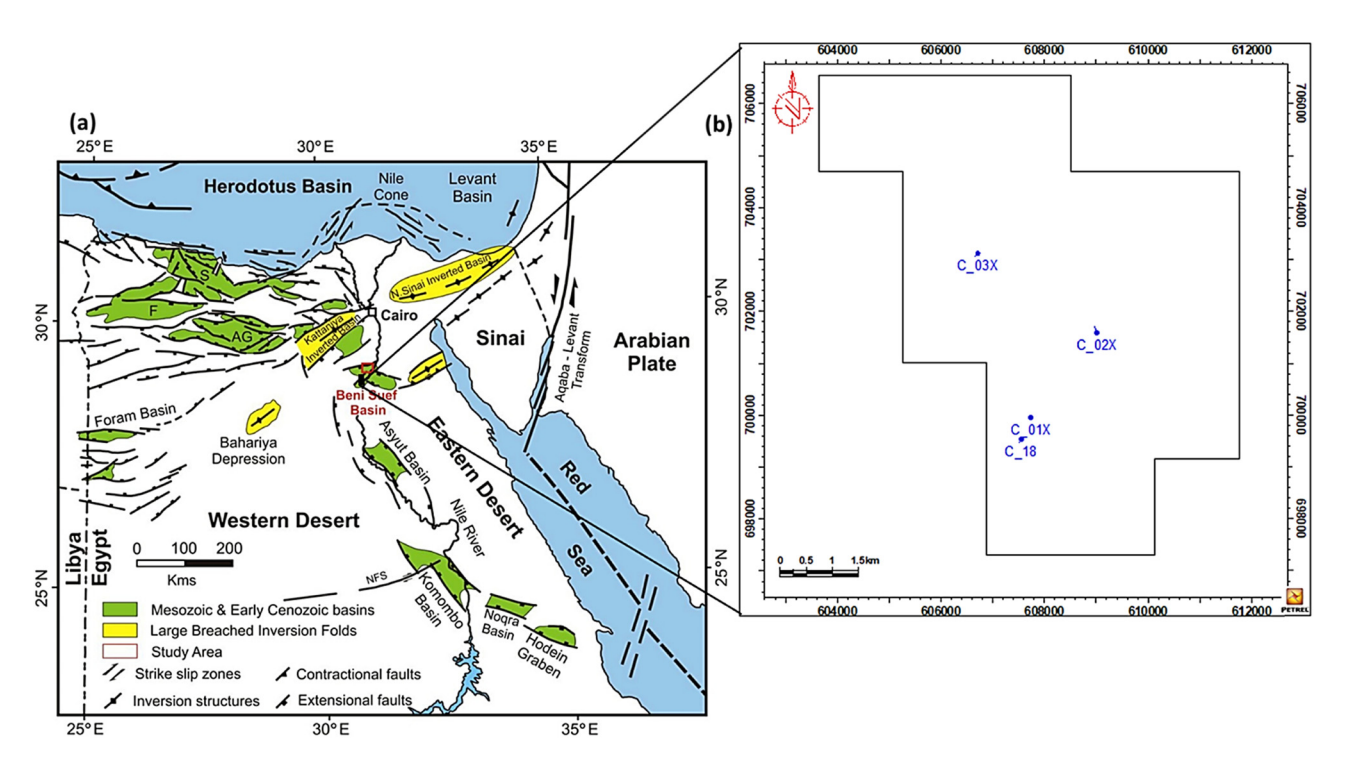


Figure 1: (a) Egypt's sedimentary basins and their major structures. AG stands for Abu-Gharadig basin, F stands for Faghur basin, and S stands for Shushan basin. The Nubian fault system depicts the study area's location after Bosworth et al. [5] and (b) the location of the wells.

Company (QPC), despite the fact that the region is quickly becoming one of the highest oil-producing provinces in Egypt [6]. Table 1 shows a brief history of the following four wells in the study area, including the selected well (WON C-3X well) for geochemical analysis.

Hydrocarbons that originated from the Albian L-Kharita (shales and siltstones) and Turonian Abu-Roash F (carbonates) are presently believed to be expelled and moved through up-dip structural closures along the basin's margins [7]. The profitable hydrocarbon source rocks in the BSB are the Kharita and Alam El-Buieb formations, which have a fair-to-good hydrocarbon potential with mainly oil and gas generation potential. It, therefore, corresponds to the basin's essential productive sources [8].

In Egypt's Western Desert, a Mesozoic petroleum system is expected to be active [1,9,10]. Generally, Mesozoic source rocks and reservoirs within the basin contemporary synchronize tectonics of the Neo-Tethyan margin period. The oil generated and expelled hydrocarbon (HC) trapping during the Jurassic periods by rotating fault blocks and cretaceous inversion antiform-like dome structures. The compressive Senonian event overturned existing extensional grabens, leading to form these antiform structures [8,11].

The source rock is a sedimentary rock of one or mixed components of shale, limestone, and/or marls that possess a high concentration of organic matter (OM). To achieve the richness of OM in the sediment in its primary depositional stages, a moderate-to-high influx of OM must be controlled by the deposition processes in anoxic conditions and a low sedimentation rate [12,13]. Therefore, the sedimentary rock that can expel a commercial amount of oil and/or gas is considered as a source rock where the classification of the source rock is based on potentiality (immature, mature, or postmature) and the OM (quality and quantity) plus the thermal maturity rate [14,15].

Accordingly, the purpose of this study is to evaluate the source rock nature, distribution, quality, and maturity and to classify the source rock intervals through cumulative depths reaching 442 m in vertical thickness of the studied well from the viewpoint of petroleum geochemistry. The geochemical analysis involves an evaluation of three sedimentary rock units. The Lower-Cretaceous shale of the Lower-Kharita (attain 149.96 m in vertical thickness) and the Upper-Cretaceous of Abu-Roash F and G (attain 305.41 m in vertical thickness). The detection of oil threshold depth, time of expulsion, and burial history modeling is illustrated in this study to give a general view for the further exploratory well of the interesting studied basin.

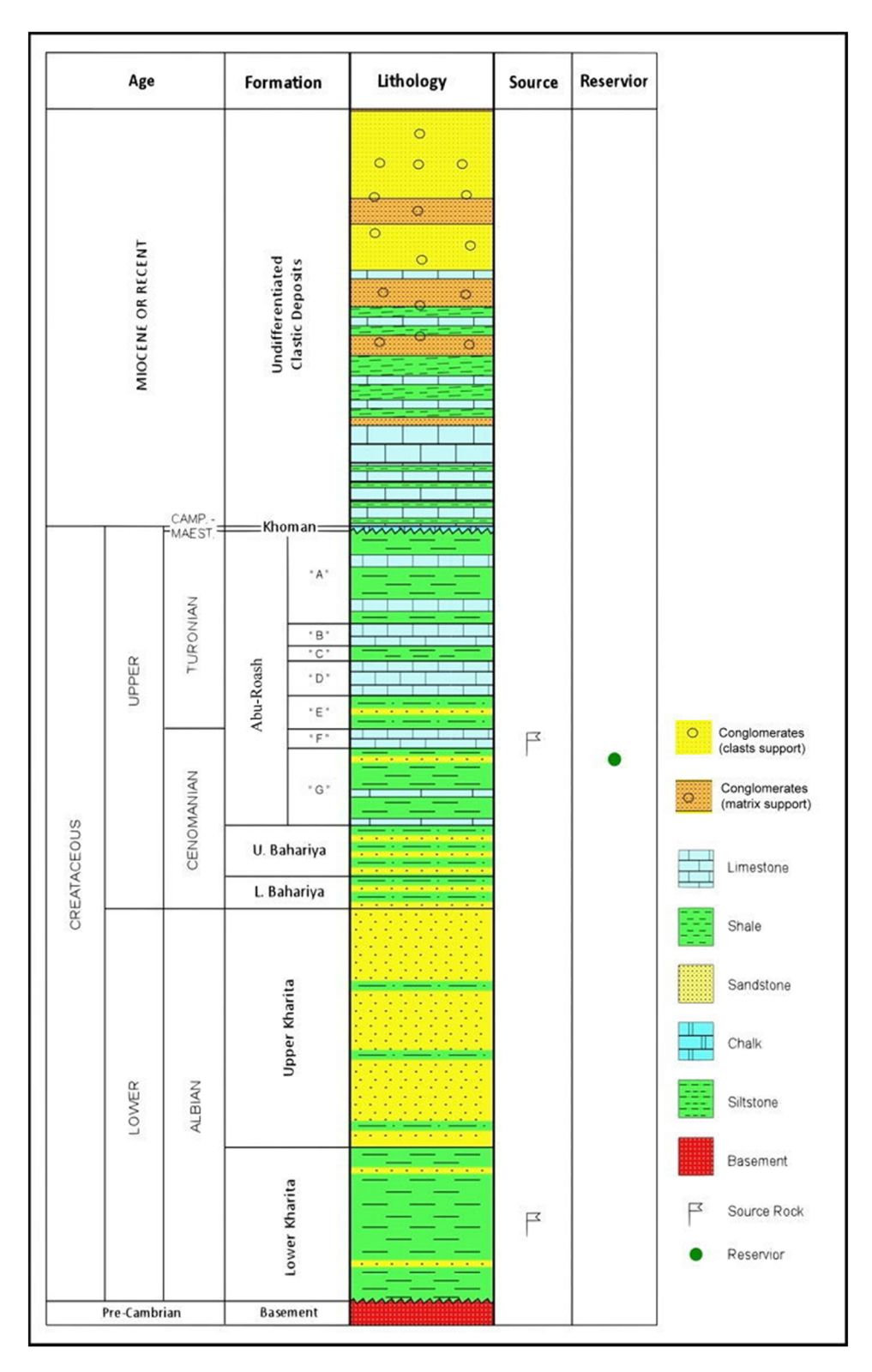


Figure 2: The sequence of lithostratigraphic units of the WON C-3X well, BSB.

Table 1: A summary of the main four wells in the study area

Well	Drilling/company	Total depth (m)	Pay zone/estimated rate
WON-C-1X	March 2011/QPC	3738.98	2.74 m pay zone and tested oil in Abu-Roash G sand with an estimated rate of 298 BOPD
WON-C-3X	September 2012/QPC	3535.68	3.04 m pay zone and tested oil in Abu-Roash G sand with an estimated rate of 450 BOPD
WON-C-2X	April 2013/QPC	3596.64	2.89 m pay zone and tested oil in Abu-Roash G sand with an estimated rate of 170 BOPD
WON-C-18	June 2014/QPC	2048.86	The well-tested oil in Abu-Roash G sand with an estimated rate of 110 BOPD

#### 2 Geological setting

#### 2.1 Stratigraphy

In the BSB, six different subsurface rock units have already been recorded [7] (Figure 2). These units are unconformably laying on the Precambrian complex of igneous and metamorphic rocks. The Albian Kharita Fm [16] considered the lowest rock units that overlay the basement and underlay the Early-Cenomanian Bahariya Fm. Kharita Fm is distinguished into two different lithologic members of L-Kharita Mb composed of siltstone with minor shale and the U-Kharita Mb composed of inter-beds of sandstone with minor siltstone inter-beds. The Baharya Fm is composed mainly of siltstone and sandstone intercalated with a streak of either shale and/or limestone [16].

The G, F, E, D, C, B, and A members of the Late Cenomanian-Santonian Abu-Roash Fm are informally distinguished into clastic terrigenous sediments of members A, C, E, and G, whereas members B, D, and F are mostly composed of carbonates and marls. The Khoman Formation, which is eroded in the present well, is characterized by chalk and lime mud with abundant chert bands of the Campanian-Maastrichtian period. Undifferentiated nonclastic to clastic sediments are deposited on unconformity upper surface of Abu-Roash and represent a marine to the Nile fill sediments of Miocene-Recent in Age?

#### 2.2 Regional structural setting

The BSB is a promising oil province, and it is the subject of various geological studies by several scientific researchers and oil companies, and several studies have been published on the hydrocarbon potentialities of different subsurface formations in the North Western Desert. All these studies have shown that the potential source rocks are widespread in space and time. Most results confirmed that the potential

source rocks and reservoirs for oil and gas are the Jurassic and Upper Cretaceous formations.

The BSB is an intracontinental rift basin that developed during the Early Cretaceous period as Western Gondwana broke up and the South and Equatorial Atlantic Oceans opened up [3,4,8]. Along the Nile river, this basin formed within Egypt's unstable shelf [16]. The Kharita Formation is mainly responsible for the thick deposits that fill this basin (1,350 m in total). These fluvial sediments (distributed through a series of half-grabens) are believed to have formed during an Early Cretaceous (Albian) period of extensional tectonics that resulted in a rift-related major subsidence [2]. The clockwise rotation of Central and North Africa was most likely the cause of extensional tectonics across the wider domain [17]. The BSB underwent a process of minor folding during the Senonian, with extensive folds and faultrelated folds, which formed during a pulsed tectonic movement of the Syrian Arc's southwest remote arm [4,18,19]. The sequencing and tectonic deformation characteristics are very similar to the Syrian-Arc folding phase tectonic structures found across many Western Desert oil fields [3,20].

At the northwestern end of a series of NW-SE-oriented Cretaceous basin systems, the BSB extends across the Nile from Egypt's Western Desert to the Eastern Desert [20,21]. The East BSB is a broad graben system bounded on two sides by NW-SE bounding faults [18].

Numerous Jurassic rift basins developed as a result of rifting caused by the splitting of the North Africa/Arabia plate from Europe [22]. Throughout the rifting process, the Syrian Arc system formed due to NW to North-Northwest-Southest (NNW-SE) to South-Southeast (SSE) shortening that adversely affected Egypt as a consequence of the closure of Neo-Tethys resulting from the convergence of African/Arabian and Eurasian plates during the Late Cretaceous. These forces resulted in the formation of North-East (NE) to East North East (ENE) trending folds that spanned Turkey, Egypt, and NE Libya [20]. The Syrian Arc folds are particularly well documented in North Sinai and the North-Western Desert [23].

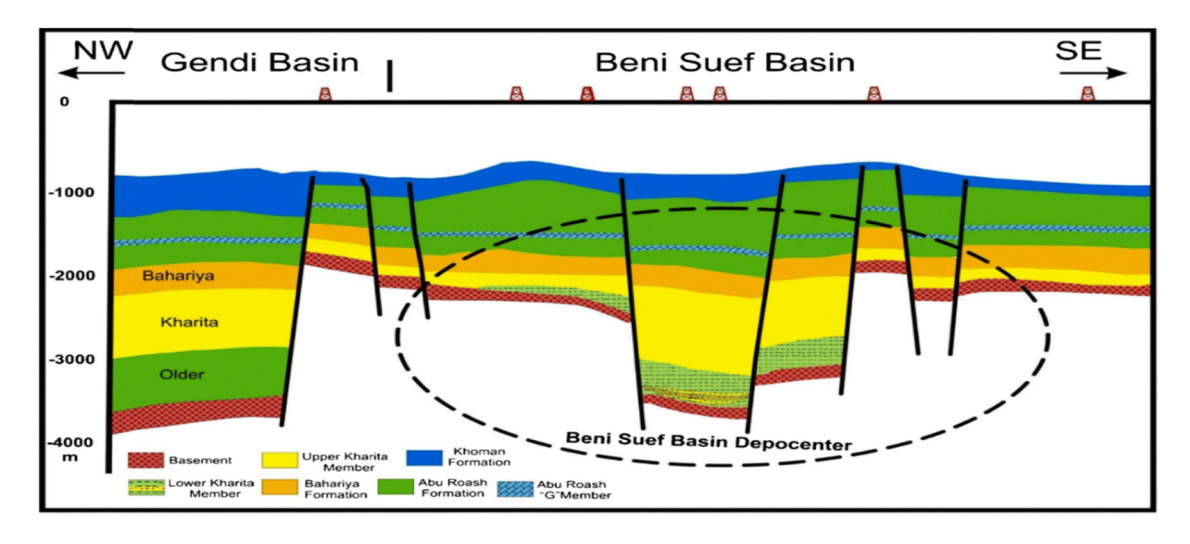


Figure 3: Regional geological cross section trending NW-SE passing through the BSB (modified after El Batal et al. [25]).

The Azhar-A2 well, with a maximum accumulated stratigraphic thickness of up to 4,000 m and a complete stratigraphic succession of the Early Cretaceous (Albian) Kharita Formation, became the trough of the BSB [24] (Figure 3).

#### 3 Materials and methods

A geochemical data set analysis, including total organic carbon (TOC), Rock-Eval pyrolysis (S1, S2, S3, and  $T_{\rm max}$ ), and a few of vitrinite reflectance measuring ( $R_{\rm o}$ ) through the exploratory WON C-3X well of a concession of west BSB, were analyzed and interpreted under the permission of the Egyptian General Petroleum Corporation (EGPC).

#### 3.1 Sampling

A cutting sample from two-interval depths between 1982.71 and 2284.48 m and from 3363.47 to 3503.68 m was collected for geochemical analysis. The sampled interval is picked up, each 3.04 m  $\approx$  10 ft. The upper interval involves the Abu-Roash F expressed by 13 cutting samples and Abu-Roash G considered by 49 cutting samples, whereas the lower interval represented particularly the older lower Kharita shale of 47 cutting samples. All sample numbers are in descending order from top to base for each representative member.

Approximately 100–200 mg of each sample was washed in distilled water to remove any contamination. Then the samples were placed to dry at room temperature (25°C) to

prohibit any loss of hydrocarbon. The samples were crushed and pulverized to 40 mesh (0.420 mm) and settled and stirred in a beaker with 10% dilute HCL for 1 h to eliminate any carbonate contents in the specimen. Heating to 70°C was applied for carbonate-rich samples like limestone and dolostone. After discarding the carbonates, a subsequent filtration and drying of powdered samples for the next geochemical analysis were required.

#### 3.2 Total organic carbon

After the removal of inorganic carbon in samples, a semi-quantitative analysis was conducted based on a combustion technique of 1 g of sample powder in Leco crucible at 1,200°C in an oxidized atmosphere. The dissolved and undissolved organic carbon was converted to gaseous state of CO and  $\rm CO_2$  that measured its amounts by infrared detector and sensor. The results of the organic carbon were calibrated and converted to be expressed in weight percentage. The TOC for present samples was measured by using an infrared-based instrument of Leco C230 system.

#### 3.3 Rock-Eval pyrolysis

Pyrolysis is a very important technique that simulates the nature condition of maturation that affects the source rock by increasing the temperature. It is conducted by continuous heating of 65 mg of powdered samples at an inert stream of helium gas with approximately a constant rate of 25°C/min from 300 to 650°C. The gases produced

during the continuous heating are measured by a flame ionized detector (FID) [14,26].

Source Rock Analyzer<sup>TM</sup> pyrolysis is the instrument used in this study to measure the quantitative amount of hydrocarbon released during each stage of sample heating. The results obtained are the amount of free hydrocarbon (S1; milligram of HC per gram of rock) and the amount of thermal cracking yield of solid OM (S2; milligram of HC per gram of rock), both detected by FID.  $T_{\rm max}$  is the maximum peak temperature of thermal cracking involved in the S2 curve that is corresponding to a maximum thermal HC yield, whereas S3 is the amount of CO<sub>2</sub> that was released from the pyrolysis of the kerogen (S3; milligram of CO<sub>2</sub> per gram of rock) and detected by IR detector.

Besides the important parameters measured directly from the pyrolysis technique, other calculated parameters based on many researchers are considered for the determination of quantity, quality, and state of maturation of source rock and are applied in the studied well [12,27–30]. Parameters used for the determination of the kerogen quantity are genetic potential (GP = S1 + S2), migration index (MI = S1/TOC), and oil saturation index (OSI = S1 × 100/TOC). Other parameters used to determine kerogen quality are hydrogen index (HI = S2/TOC × 100), oxygen index (OI = S3/TOC × 100), and S2/S3. The maturity state is mainly used to calculate the parameter of production index (PI = S1/[S1 + S2]) with  $T_{\rm max}$ .

Because of a limited number of  $R_o$  measuring samples for the studied well, the calculated  $R_o$  is instead the true measurement, applying to cover a wide range of studied geochemical analysis based on the equation postulated by Jarvie et al. [29] ( $R_o\% = (0.0180 \times T_{max}) - 7.16$ ).

The relative hydrocarbon potential (RHP) = (S1 + S2)/TOC [31] versus depth and applying correlation coefficient and regression linear equation between the  $R_o$  against burial depth by statistical analysis of two variants using Origin Pro v.15 software is used to determine expulsion threshold depth and active source rock limit depth. Also, either Origin Pro or Corel Draw photo software suit v.12 is used for cross plot samples in this study figures. Burial history diagram and petroleum system are carried out by using Petromode software v11.

#### 4 Results and interpretations

According to the studied geochemical analysis, the 109 cutting samples involve three informal rock units from top to base: the Abu-Roash F (27.13 m; from depth 1990.64

to 2017.77 m), Abu-Roash G (278.28 m; from depth 2017.77 to 2296.05 m), and L-Kharita (149.96 m; from depth 3358.28 to 3508.24 m). Hence our results are to consider the geochemical properties of these three important rock units as shown in Table 2.

#### 4.1 Quantity nature of OM

The TOC analysis of the studied rock units shows a significant variety. It ranges from 0.53 to 2.78 (average 1.26 wt%) for Abu-Roash F with gradual increase in the TOC contents towards the base of this unit. Abu-Roash G is characterized by TOC of 0.52–2.77 (average 0.93 wt%) and 0.56–1.81 (average1.22 wt%) for L-Kharita (Table 2). The free hydrocarbon S1 is 0.04 at the top of the Abu-Roash F, increasing slightly to reach 1.25 at the base (average 0.43 mg HC/g rock). These S1 values represent high contents of 1.09 at the uppermost part of Abu-Roash G and obviously decrease in the entire sedimentary unit to record their minimal amounts of 0.05 near its base with an average of 0.18 mg HC/g rock. The L-Kharita has an average of S1 amount equal to 0.3 mg HC/g rock within the range of 0.09–0.92 (Table 2).

A migration index (MI = S1/TOC), according to Smith [32], shows that all samples have MI values between 0.07 and 0.74 for all studied samples that refer to indigenous hydrocarbon habitat. The OSI for the same stratigraphic units is within the range of 7.47–74.13, with an average value of 27.35, 15.49, and 24.05, respectively, for the studied rock units from the top to the base (Table 2). All measured samples have values of OSI <74.31. The plotted diagram of 109 studied samples upon the S1 versus TOC diagram of Jarvie et al. [29] illustrates that all samples lay within the area of an indigenous hydrocarbon with no contamination (Figure 4).

The generated cracking HC S2 for the studied rock units shows that the Abu-Roash F shows increasing values from 0.05 at the top reaching 17.35 at the bottom with an average value of 7.08 mg HC/g rock. The Abu-Roash G exhibits S2 values from 0.41 to 2.78 with an average value of 2.35 mg HC/g rock, and L-Kharita of S2 values ranges from 0.5 to 2.49 with an average value equalling 1.25 mg HC/g rock.

The S2 versus TOC diagram of Peters and Cassa [27] shows that the Abu-Roash F samples lay within the three zones of cracked generated HC of fair (46.15%; 6 samples), good (30.77%; 4 samples), and very good (23.07%; 3 samples) (Figure 5). The other samples of Abu-Roash G and L-Kharita are set within the fair and good cracked generated

**Table 2:** Summery of Rock-Eval pyrolysis data and indices of Abu-Roash F, Abu-Roash G, and L-Kharita members, WON-C-3X well

Rock units	Depth interval (m)	Thickness Total (m) sampl	Total samples	Values	TOC (wt% of rock)	S1 (mg HC/g rock)	S2 (mg HC/g rock)	S3 (mg CO <sub>2</sub> /g rock)	GP = S1 + S2 (mg HC/g rock)	S2/S3 (mg HC/ mg CO <sub>2</sub> )	HI (mg HC/ g rock)	OI (mg CO <sub>2</sub> /g rock)	T <sub>max</sub> (°C)	Ro calc. (%)	PI = S1/(S1 + S2)	Heat flow calc.
Abu- Roash F	1990.64–2017.77 27.13	27.13	13	Minimum Maximum	0.53	0.04	0.5	0.42	0.54	0.85	95	33	428	0.54	0.04	84.65
-				Average	1.26	0.43	7.08	0.95	7.51	99.9	336	71	432	0.62	0.06	90.11
Abu- Roash G	2017.77–2296.05 278.28	278.28	49	Minimum Maximum	0.51 2.77	0.04 1.09	0.41 15.79	0.4 1.64	0.51 16.88	0.38 18.15	76 570	31 176	429 445	0.58 0.83	0.05	85.71 94.67
				Average	0.93	0.18	2.35	0.61	2.54	3.34	180	78	438	0.73	0.09	93.06
ٺ	3358.28-3508.24 149.96	149.96	47	Minimum	0.53	80.0	0.5	0.33	0.58	9.0	9/	33	448	6.0	0.11	93.72
Kharita				Maximum	1.81	9.0	2.49	1.09	3.09	3.93	145	151	465	1.21	0.28	95.12
				Average	1.22	0.3	1.25	0.47	1.55	2.09	101	22	458	1.09	0.19	94.55

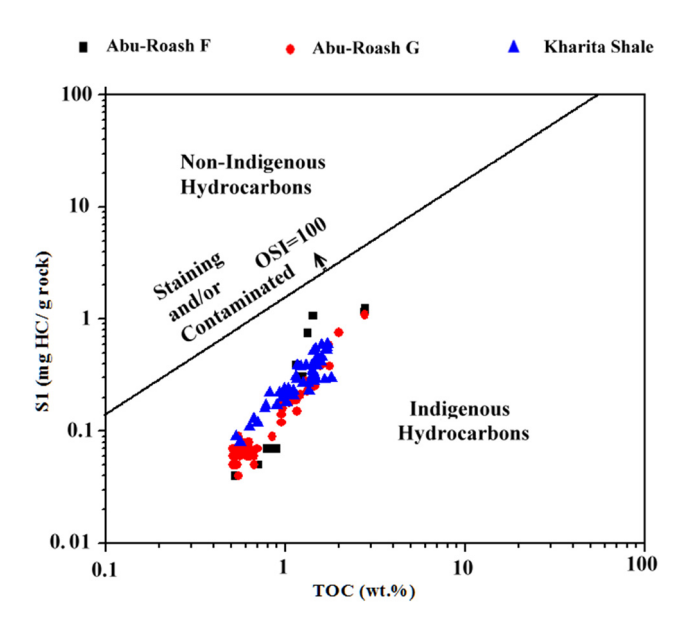


**Figure 4:** Cross plot of S1 versus TOC diagram of the studied rock units [29].

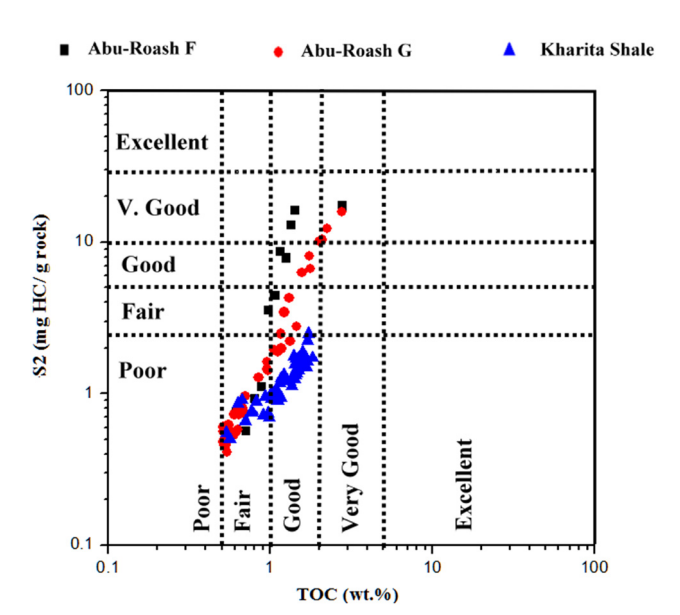


**Figure 5:** Cross plot of the S2 versus TOC diagram of the studied rock units [27].

HC. The samples of Abu-Roash F exhibit both fair (69.38%; 34 samples) and good (30.62%; 15 samples) cracked generated HC. The L-Kharita samples exhibit a better position than Abu-Roash G in the diagram, showing fair (25.53%; 12 samples) and good (74.46%; 35 samples) cracked generated HC (Figure 5).

GP of the studied samples is counted, according to Hunt [12], into four categories as follows: poor (<2), fair (2–5), good (5–10), and very good (>10). The Abu-Roash F

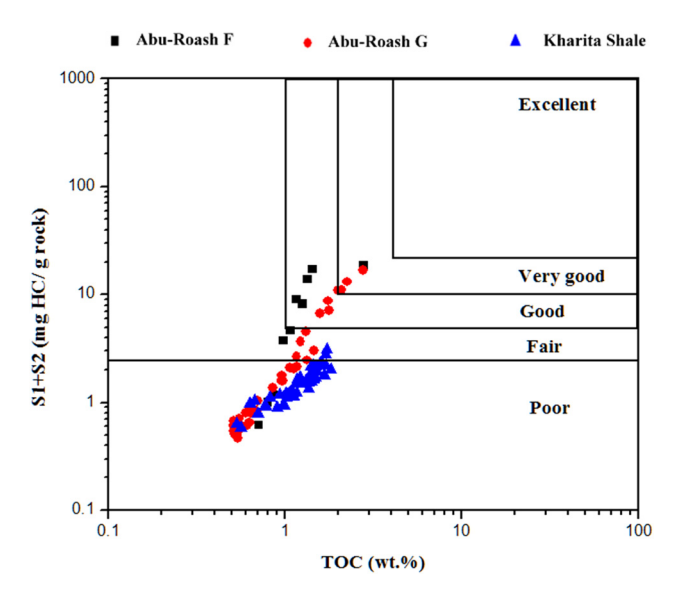


**Figure 6:** Plot diagram of GP versus TOC of the studied rock units showing the generating potential of studied rock units [34].

has five samples of GP <2 representing 38.46%, two samples of fair (15.38%), two samples of good (15.38%), and four samples of very good (30.76%). The GP of the Abu-Roash G is dominated by 34 samples of poor (69.38%), 8 samples of fair (16.32%), 3 samples of good (6.12%), and 4 samples of very good (8.16%). L-Kharita has GP of both dominant poor 76.59% (36 samples) and fair 23.4% (11 samples; Table 2).

Cross plot of the samples at the GP versus TOC diagram of Vandenbroucke and Largeau [34] shows that the potential of HC generation of almost all samples of the Abu-Roash F and L-Kharita fit in the poor area of the diagram in Figure 6. Two samples (4.25%) of L-Kharita are plotted in the fair area of the same diagram. Nine samples (18.37%) of Abu-Roash G are scattered in areas of fair, good, and very good (Figure 6), whereas eight samples (61.53%) of Abu-Roash F have a GP range from 3.75 to 18.5 plotted in the areas of very good, good, and fair (Table 2). The rest five samples (38.46%) of Abu-Roash F are laid within the poor area absolutely from the uppermost part of the rock unit.

#### 4.2 OM genetic types

Five categories of kerogen types are distinguished in this study based on two parameters: HI (<50, 50–200, 200–300, 300–600, and >600) and S2/S3 ratio (<1, 1–5, 5–10, 10–15, and >15) according to earlier studies [15,27]. They are types IV, III, II/III, II, and I of non-, gas-, gas and oil-, oil-, and oil-prone HC in the respective order.

Based on HI, the Abu-Roash F shows four categories of kerogen types of III (38.46%; 5 samples), II (30.76%; 4 samples), I (23.07%; 3 samples), and mixed type II/III (7.69%; 1 sample), whereas the Abu-Roash G shows three kerogen categories of type III (79.59%; 39 samples), type II (16.32%; 8 samples), and type I (4%; 2 samples). All of the samples from L-Kharita rock units belong to type III (100%; 47 samples) (Table 2).

Based on the S2/S3 ratio, the Abu-Roash F shows five categories of kerogen types from descending percentages: II/III (38.46%; 5 samples), II (23.07%; 3 samples), I (15.38%; 2 samples), IV (15.38%; 2 samples), and I (7.69%; 1 sample). The Abu-Roash G also shows five categories of kerogen types. From a descending percentage, they are types III (63.26%; 31 samples), IV (20.4%; 10 samples), II/III (8.16%; 4 samples), II (4.08%; 2 samples), and I (4.08%; 2 samples). The samples from L-Kharita exhibit a dominance of type III (87.23%; 41 samples), whereas the rest of samples belongs to type IV (12.76%; 6 samples; Table 2).

In this study, the pseudo van-Krevelen diagram is used to identify types of kerogen according to also Vandenbroucke and Largeau [34], in which, the HI versus OI is used instead of the original H/C versus O/C atomic ratios (Figure 7).

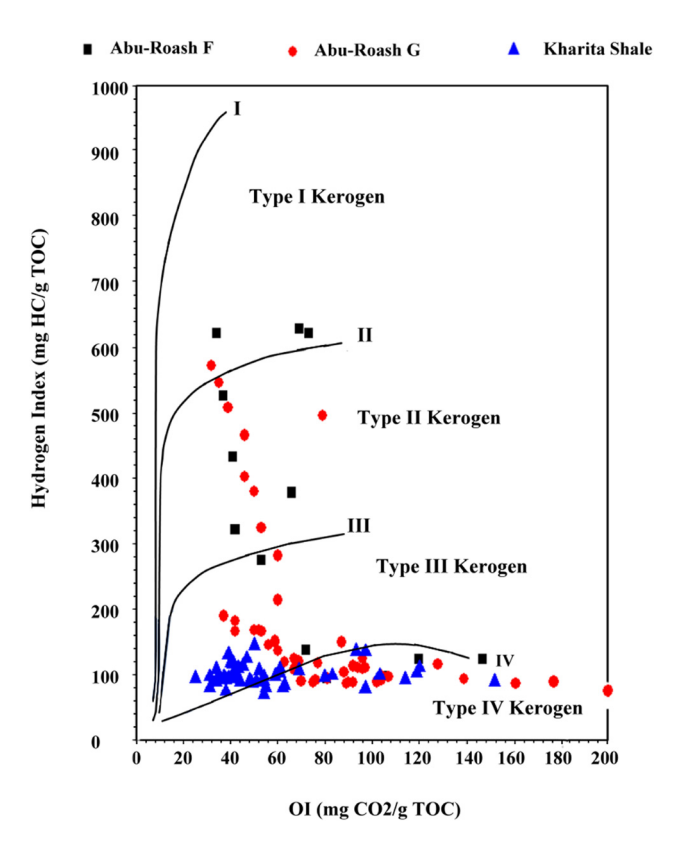


Figure 7: Pseudo van-Krevelen diagram shows a dominated type of kerogen in the present rock units [34].

The representative samples plotted on the HI versus OI diagram exhibit that the Abu-Roash F samples fit in the area of type II (38.46%; 5 samples), types I and II of equal percentages (23.07%; 3 samples for each of them), and type IV (15.38%; 2 samples). The Abu-Roash G characterized by fall samples within the field of type IV (46.93%; 23 samples), type III (36.73%; 18 samples), type II (14.28%; 7 samples), and type I (2%; 1 sample). The L-Kharita shows a mixture of type III (59.57%; 28 samples) and type IV (40.42%; 19 samples).

The plotted studied samples on the S2 versus TOC, according to Langford and Balanc-Valleron [35], show that the Abu-Roash F has a variety of types I, II, and III kerogen that amounts to 23% (3 samples), 30.77% (4 samples), and 46% (6 samples), respectively. The samples belong to Abu-Roash G show a variety of type I (14%; 7 samples), mixed type II/III (22.48%; 11 samples), and type III (63.26%; 31 samples). The L-Kharita rock unit exhibits a unitype of kerogen where all samples set within area of type III kerogen (Figure 8).

Two diagrams are selected to plot the studied samples regarding the different rock units based on their amounts of HI and TOC. The first is according to Walters [13] that combined the atomic H/C ratio in the same diagram and the other by Delvaux et al. [36] focusing on the type of hydrocarbon generated from the source rocks. Accordingly, from the Abu-Roash F, one sample fits in the area of good potential (7.69%), five samples plot in the area of moderate potential (38.46%), and seven samples plot in the area of poor potential (53.84%). From them, 53.84% (seven samples) within the band of oil prone and 46.15% (six samples) are plotted in band of gas-oil prone.

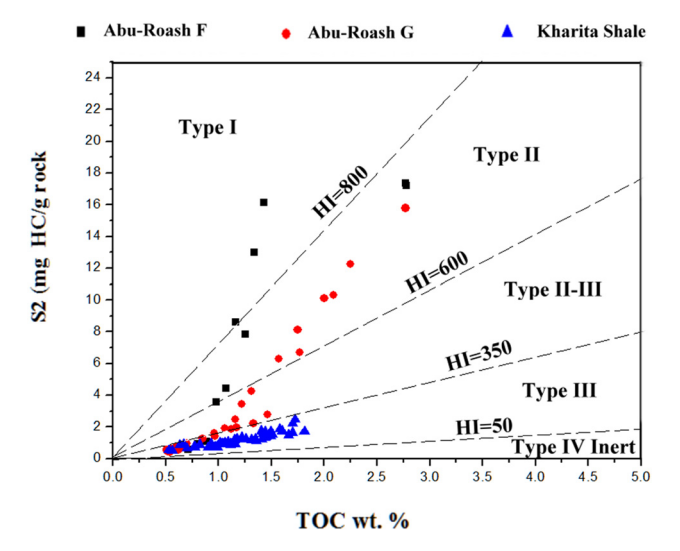


Figure 8: Cross plot of S2 versus TOC shows the kerogen types of the studied rock units [35].

A study by Walters [13] distinguishes seven types of kerogen; according to the author, the studied samples of 1–1.2 atomic H/C ratio including all samples of L-Kharita and some of Abu-Roash G belong to type IIIC kerogen of primarily vascular land plant and algae that were deposited in coastal plains (oil-prone coals). The other set of samples of H/C ratio between 1.2 and 1.4 of Abu-Roash G and F indicates the marine algae and plankton origin and is found within marine shale type II and type IIS within marine carbonated and silicates.

As the same as from the diagram (Figure 9b), the Abu-Roash F samples set within the areas of good-oil source (38.46%; 5 samples), fair-oil source (61.53%; 8 samples), and gas-oil source (15.38%; 2 samples).

Similarly, the Abu-Roash G samples exhibit a variety of good (8.16%; 4 samples), moderate (22.44%; 11 samples), and poor (72.34%; 34 samples) source potentials. From them, 14.28% (7 samples) were set within the field of oil prone and 85.71% (42 samples) within the field of gas-oil prone (Figure 9a). Figure 9b shows that the Abu-Roash G samples are laid within bands of fair-oil source (69.38%; 34 samples) and gas-oil source (30.61%; 15 samples). The L-Kharita samples laid within the poor and moderate potentials of 25.53% (12 samples) and 74.46% (35 samples), respectively. L-Kharita samples are situated in the area of gas-oil prone. The L-Kharita samples dominate gas-oil sources of 89.36% (42 samples) to 100% (47 samples) as shown in Figure 9a and b, whereas 10% (5 samples) of L-Kharita exhibit a fair-oil source (Figure 9b).

#### 4.3 The rate of OM maturity

The degree of metamorphism act on OM in the source rock can be determined by some indexes like the  $T_{\rm max}$ , PI, and  $R_0$ . The thermal maturity as a function of burial depth in the basin influenced by the type of OM, MM associated, and age of source rocks [14,27,37] considers immature OM in case of PI <0.1,  $T_{\rm max}$  < 430°C, and  $R_{\rm o}$  < 0.62. If PI reaches 0.4 and  $T_{\rm max}$  reaches 450–460°C with  $R_0$  < 0.9, it characterizes the top of the oil window, while postmature OM is of  $T_{\text{max}} > 470$ °C, PI >1, and  $R_{\text{o}} > 1.35$ [27], and the condense gas (late mature OM) is in-between the oil and dry gas windows. Tissot and Welte [14] mentioned that the  $R_0$  values of the oil window are different based on the kerogen involved. The authors found that the  $R_0$  values of oil window for type I are initiated at 0.64%, peaked at 1.1%, and eliminated at 1.4%  $R_0$ , type II  $(0.5-0.8-1.4\% R_0)$ , and type III  $(0.55-0.9-1.4\% R_0)$ .

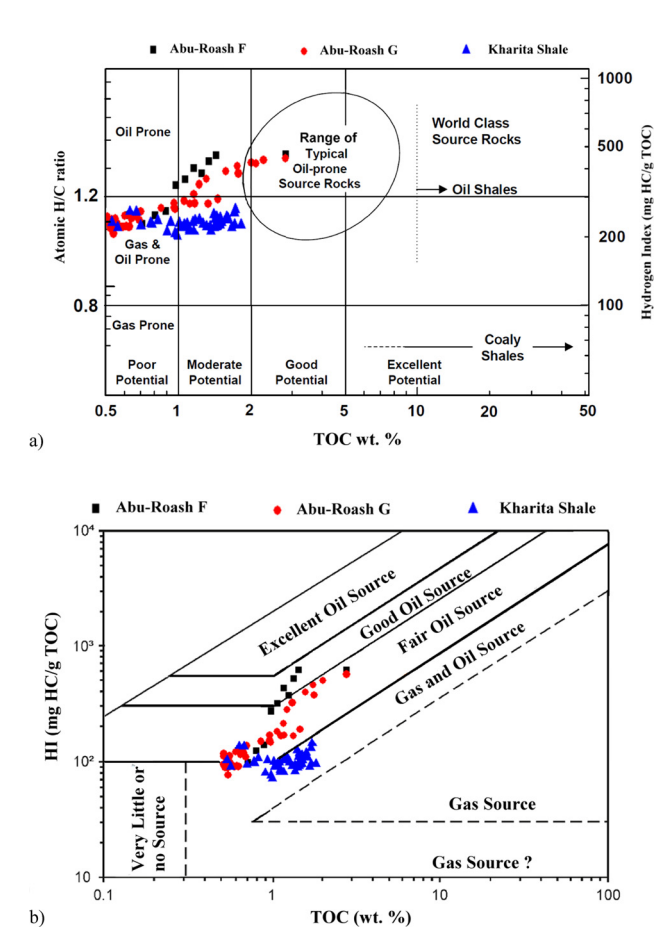
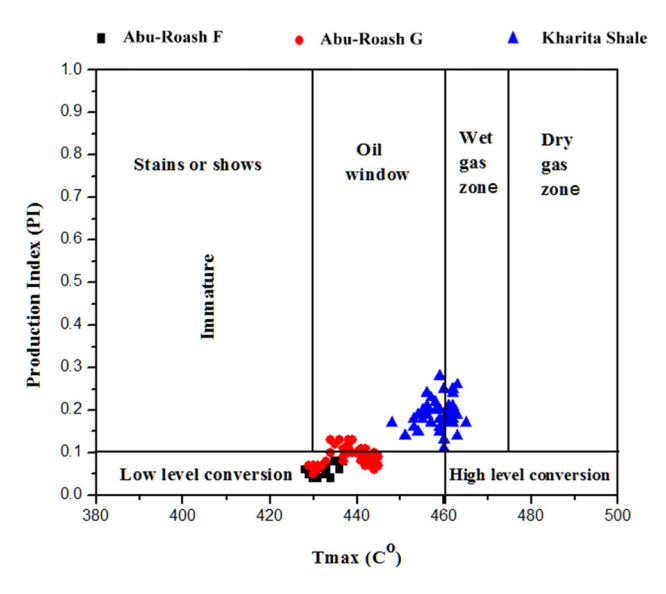


Figure 9: HI versus TOC cross plot of the studied rock units according to Walters [13] in diagram (a) and Delvaux et al. [36] in diagram (b).

 $T_{\rm max}$  of the Abu-Roash F samples has an average of 432°C within the range of 428–437°C. The Abu-Roash G has an average  $T_{\rm max}$  equal to 438°C within the range of 429–445°C, whereas the L-Kharita has  $T_{\rm max}$  within the range of 448–465°C (average 458°C). The PI of the studied samples of the Abu-Roash F has an average of 0.06, all <0.1. The Abu-Roash G shows the PI values <0.1 (63.26%; 31 samples) and >0.1 (32.65%; 16 samples), whereas the entire L-Kharita has the PI values between 0.11 and 0.28 (average 0.19). The calculated  $R_{\rm o}$  has a value progressively increasing with depths of average 0.62 (Abu-Roash F), 0.73 (Abu-Roash G), and 1.09 (L-Kharita).

Cross plot of the studied rock units on the PI versus  $T_{\rm max}$  diagram according to an earlier study [33] shows that almost all of the Abu-Roash F and G rock units lay in the mature oil window. Only 16 samples of Abu-Roash G have PI >0.1 (Figure 10). In contrast, all the samples of L-Kharita have the PI >1 to <0.3 and lay between the mature oil window (68.08%; 32 samples) and wet-gas zones (31.91%; 15 samples).



**Figure 10:** Cross plot of PI versus  $T_{\text{max}}$  shows the maturity of the studied rock units [33].

Plotting the studied samples on the similar diagram of maturity considering HI versus the  $T_{\rm max}$  [38] (Figure 11) shows that the Abu-Roash F and G rock units are plotted within the area of oil-window involved a mixture of types II and III, whereas all the samples from L-Kharita are plotted within the field of condensate-wet gas of high maturity level.

Furthermore, by plotting the studied rock units on the source rock index (SRI) chart, established by Jiang et al. [39] (Figure12), the diagram shows that all rock units have samples laying in the zones of SRI <0 characteristics for the nonhydrocarbon source rocks, whereas the other samples lay within the zones of either poor source rocks of SRI 0–25 (dominated by Abu-Roash F and G samples) or within the zones of medium source rocks of SRI 25–50 (dominated by L-Kharita samples).

# 4.4 Prediction of expulsion threshold, active source depth limit (ASDL) depths, and heat flow

Two methods were used to determine the quantitative depths in this study. The first is based on RHP versus depth ratios, according to a study by Pang et al. [31], and the other is based on  $R_o$  versus depth ratios, according to either concepts of maturity of Tissot and Welte [14] or Peters and Cassa [27] (Figure 13). The correlation coefficient between the  $R_o$  and depth shows a positive linear relationship dot line (r = 0.95, and SD = 0.06) between 109 samples (Figure 13).

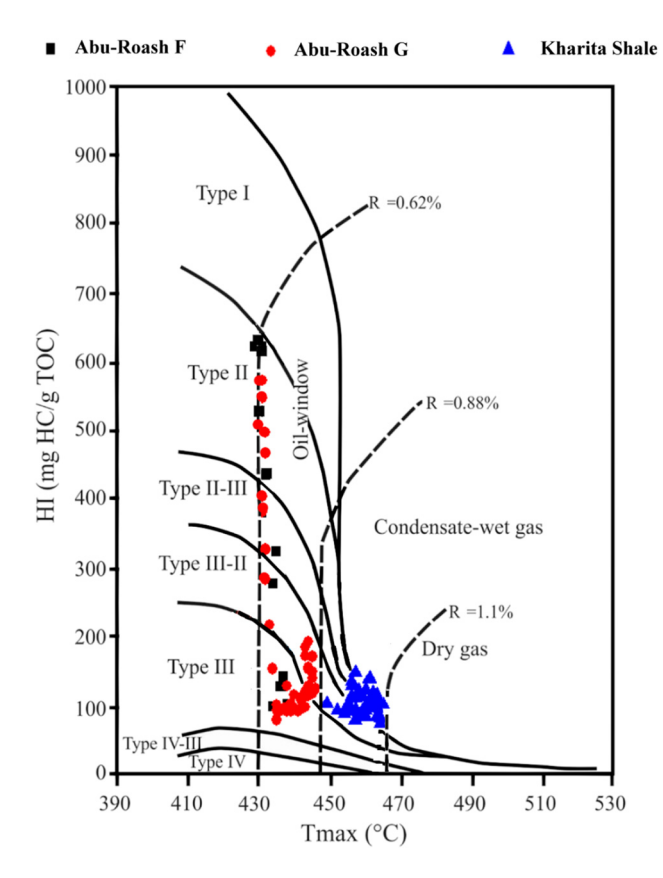


**Figure 11:** Cross plot of HI versus  $T_{\text{max}}$  shows the types and the maturity of the studied rock units [38].

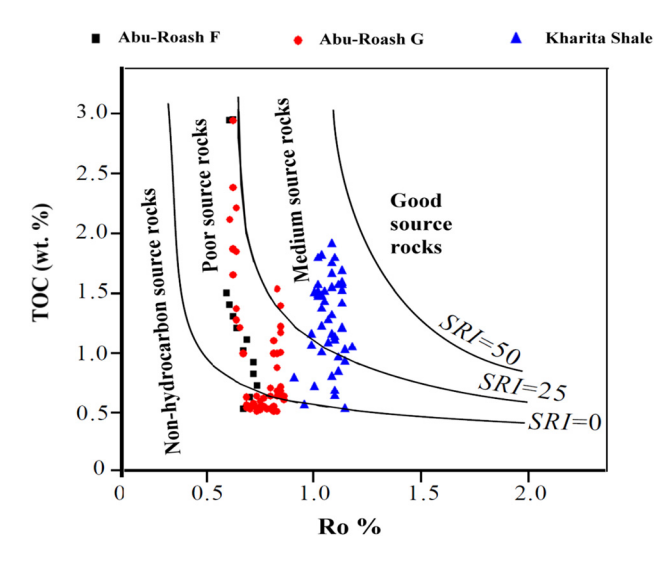


Figure 12: SRI chart of TOC versus  $R_0$  of the studied rock units [39].

Detection of threshold expulsion depth in the present study determines according to two ways; Directly from the curve of the maximum recorded value of RHP plotted against with depth according to ref. [31] (Fig. 13a). And, indirectly, were done in two steps. The first step is by

making a linear regression line between the  $R_{\rm o}$  and the depth (Fig. 13b, c). Then the authors used the suggested  $R_{\rm o}$  values for the oil window of involved kerogen type II and III according to ref. [14] (Fig. 13b) and the according to  $R_{\rm o}$  value of initial peak maturity according to ref. [27] (Fig. 13c). The result shows that the depth of 2,000 m is the proposal depth of expulsion threshold. From the same diagram (Fig. 13) the ASDL depth is directly determined as a minimum withdraw depth of the RHP curve as shown in (Fig. 13a) or as the intersection limit depth of oil window (peak mature) and condensate gas (late mature) (Fig. 13b, c). The result shows that the ASDL depth is about 2,750 m.

Moreover, Pang et al. [31] discussed the mutual relationship between those depths not only based on the burial depth and type of kerogen but also with a close effect on the rate of heat flow within the basin itself. The authors mentioned that the ASDL reduces in depth or becomes shallower, <5,500 m within the basins characterized by high-heat flow >70 mW/m<sup>2</sup>. So based on our prediction of ASDL at 2,750 m and the suggested equation of Pang et al. [31] (ASDL =  $16,202 - (2.63 \times HI) - (139.46 \times HF)$ ), we can calculate the heat flow within the studied basin. The average heat flow affected the studied rock units of Abu-Roash F (90.11 mW/m $^{2}$ ), Abu-Roash G (93.06 mW/m $^{2}$ ), and L-Kharita (95.55  $\text{mW/m}^2$ ) (Table 2). The above results confirm that the studied basin is characterized by highheat flow that plays a role in shallowing of the ADSL depth within the basin.

## 4.5 Lithology against rich and poor OM intervals

To give a more accurate interpretation of the studied source rock intervals within the well, the lithology must be shared with the geochemical data as shown in Figure 14. Our interpretation was established based on five factors for poor rather than richness horizons. Step 1 used previously plotted diagrams to separate samples of IV kerogen (Figure 7) and separate samples of SRI <0 (Figure 12) and calculated parameters of S2/S3, TOC, and also GP to separate low and intermediate horizons than the richest OM horizon. Step 2 determines the types of sediments without going into the details, and step 3 determines the maturity level. The result is ten numbers each giving a basic idea on each interval (Figure 14). The method succeeds in determining the main pay zones and the optimal rich source rock horizons in the field. The disturbance of data in previous figures by this method is clear to interpret easily. Ninety per cent of the Abu-Roash F is an

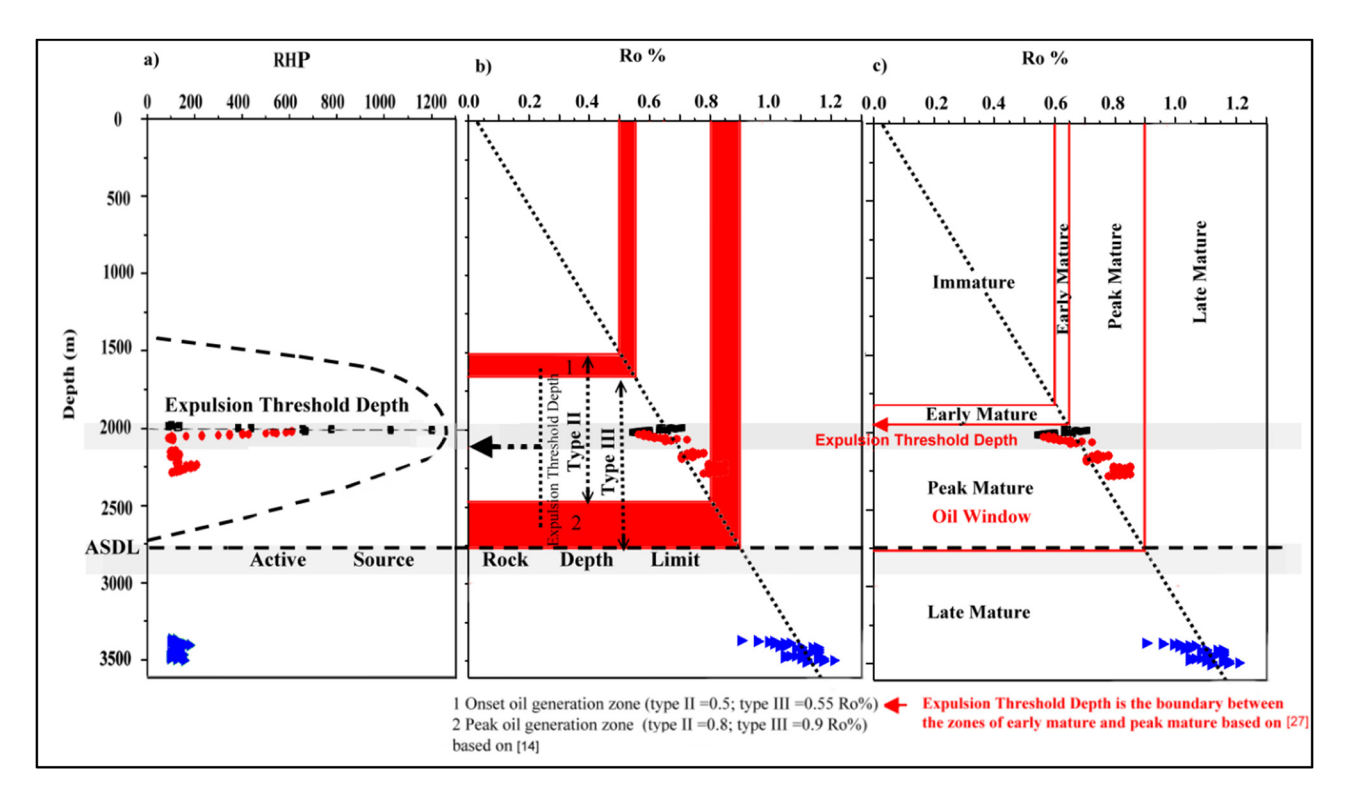


**Figure 13:** Prediction of the expulsion threshold and ASDL depths by a cross plot of depth in the studied well; (a) versus the RHP according to refs [14]; (b and c) versus  $R_0$  according to refs [27,31].

optimal organic-rich source rock of limestone, argillaceous limestone, and shale of 27.13 m thick. The rest 10% of the uppermost contact with the overlaying rock unit is considered a medium-to-low source rock ranging in maturity from early to peak mature. The Abu-Roash G is composed of three intervals: the upper rich interval from 2017.77 to 2054.35 m composed of optimal organic-rich source rock, shale, and siltstone intercalated with three separated pay zones each reaching 3-4 m in thickness. The second interval is presented by a dominant mediumto-poor source rock from 2057.40 to 2228.08 m composed of intercalations of shale, lime, siltstone, and few sandstones. The third interval at the lower part of the rock unit from 2234.18 to 2296.05 m is characterized by upper half of the optimal organic-rich source rock of shale, limestone, argillaceous lime, and siltstone decreasing to become medium and poor source at the base. At a depth of 2242.30 m, a 10 m thick sandstone represents a reservoir, but it is not produced by the present well; however, it is considered as a pay zone in other well in the field. The L-Kharita is considered an organic-rich source rock of shale and siltstone within the condensate mature zone. The middle part of L-Kharita is characterized by at least four pay zones of sandstone intercalation starting from depth 3414.7 m until 3458.45 m.

### 4.6 Burial and thermal histories of petroleum generation

The detailed construction of maturity history model of source rock intervals within the studied well is applied using one-dimensional basin-modeling Petro-mode software (Figure 15). The distribution of the thermal maturity levels of the studied basin is applied based on the Easy\%  $R_0$  [40] to determine the time when the source rocks passed through the oil window. The early oil generation for the L-Kharita had begun after 97 Ma at the depth of 1508.77 m till 93 Ma, where its upper surface reaches 158.96 m depth within paleo temperature between 92.88 and 99.24°C. L-Kharita entered the peak of oil at a time interval between 91 and 85 Ma within depth of 2072.64 and 2133.6 m, respectively, within the temperature zone of 105.59-111.94°C (Figure 15a). The late-oil zone recorded at 58 Ma where the base of the member reached to a depth of 2758.44 m at which the temperature was 124°C and ended at 7.5 Ma where its upper bedding plain match a burial depth of 3230.88 m and temperature attains 137.35-143.71°C with present-day  $R_0$  (0.9–1.21). The younger Abu-Roash G and F members, unlike the L-Kharita, only entered the early oil generation beginning with Abu-Roash G since 56 Ma at a burial depth of 1,524 m. Abu-Roash G still keeping at that

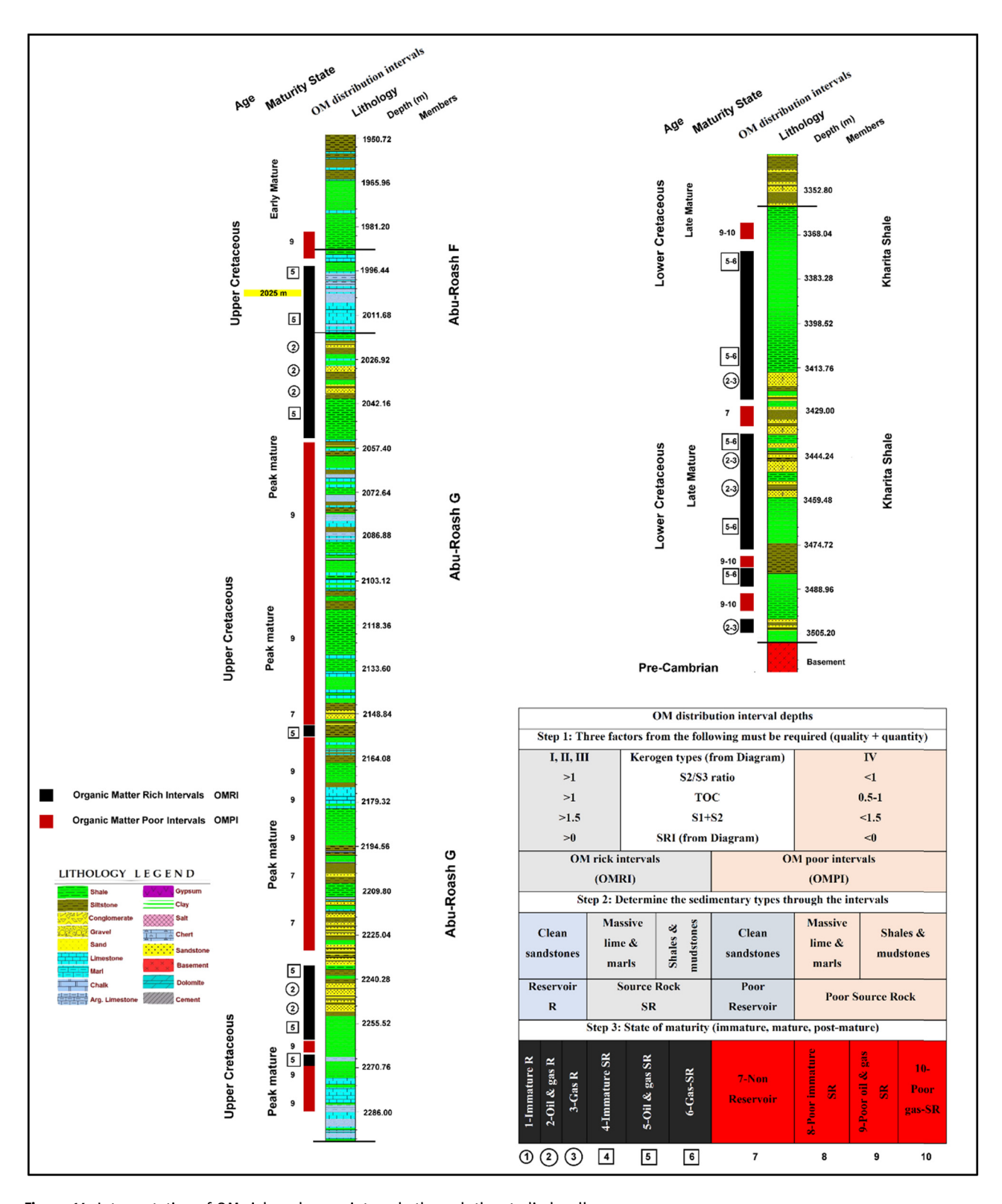


Figure 14: Interpretation of OM-rich and -poor intervals through the studied well.

stage with a slight increase at a burial depth of 1,828 m till 19 Ma, whereas Abu-Roash F entered the stage of early oil generation since 18 Ma with a burial depth of 1828.8 m.

Accordingly, the promising source rocks for oil generation in the studied well are Abu-Roash F and G where they have to enter the early stage of oil generation and

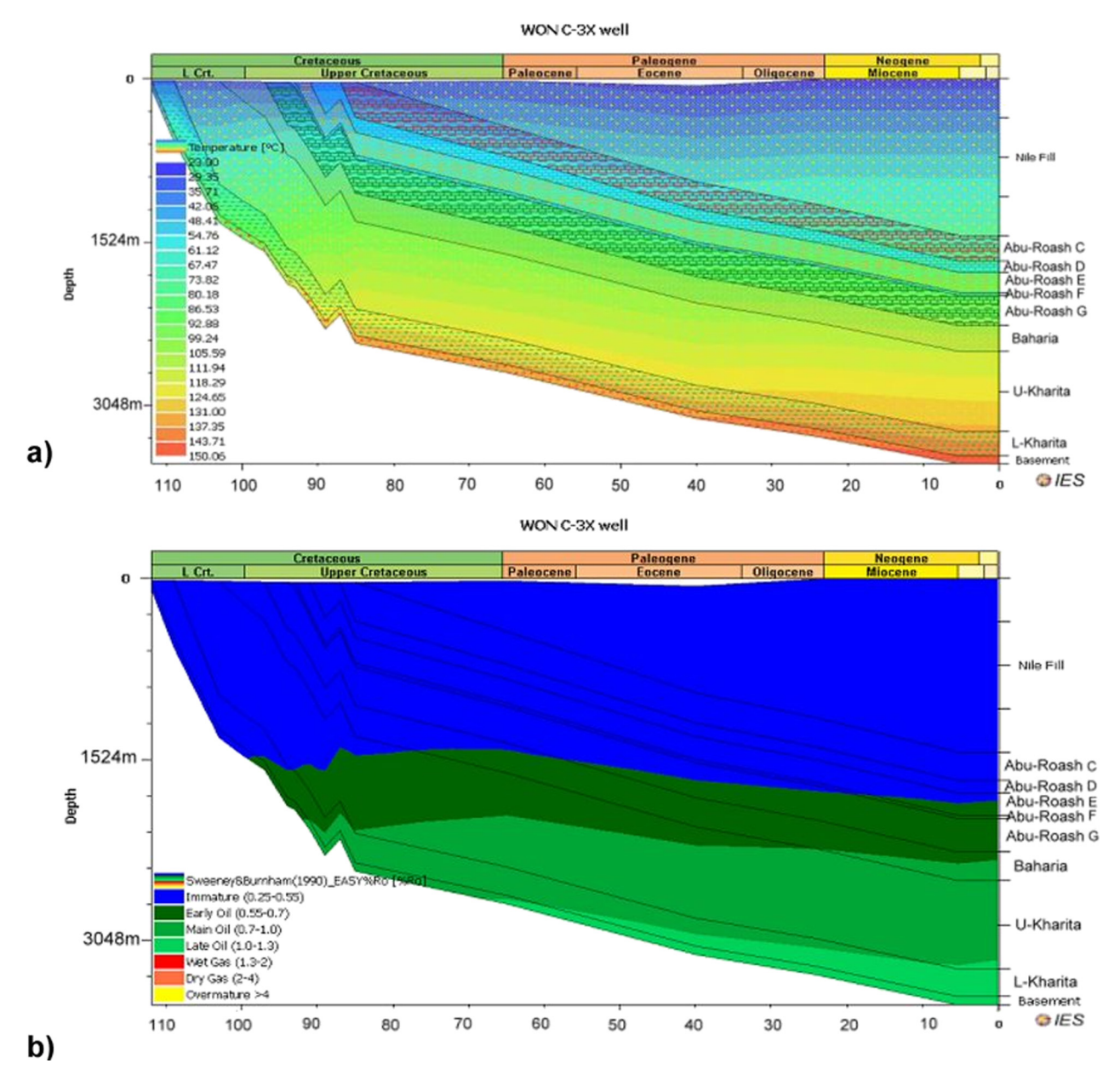


Figure 15: (a) Thermal maturity and (b) burial model of the Abu-Roash F, Abu-Roash G, and L-Kharita source rocks for the studied well.

expulsion since 56 Ma. Whereas the L-Kharita member is now at the late stage of oil and beginning of gas that refer to had been generate and expelled enough quantity of hydrocarbon during their thermal maturity history.

#### 5 Conclusion

The authors believed that the entire thickness of Abu-Roash F, Abu-Roash G, and L-Kharita and the three important rocks in the BSB are source rocks. However,

the TOC, Rock-Eval parameters and indices plus interpreted lithology from wireline logs, and OM-rich and -poor intervals set that assumption is not exactly valid. The Abu-Roash F is an optimal oil-prone source rock from an interval depth of 1997.96–2019.30 m (21.34 m) characterized by TOC of a fair-to-high reach (2.78 wt%), GP is fair to very good (3.75–18.47 mg HC/g rock), kerogen types of (II and II/III), and HI values within the range of 321–619 mg HC/g TOC of mostly deltaic and/or marine setting. This source rock represents 78.66% of the entire thickness of the Abu-Roash F that attain 27.13 m. The Abu-Roash G is a huge thick rock unit in this study to

attain 278.28 m and also to contain two categories of source rock of oil prone at the interval of 2019.3-2049.78 m (30.48 m) and of oil-gas prone at the interval of 2235.71-2254 m (18.29 m). The upper source rock of Abu-Roash G is 30.48 m characterized by TOC of fair to high (1.16-2.77 wt%), GP of fair to very good (2.67-16.88 mg HC/g rock), kerogen types of (II-II/III), and HI values within the range of 324-570 mg HC/g TOC of mainly deltaic and marine origin. The lower source rock interval of the same member is 18.29 m distinguished by TOC of fair to good (0.96-1.46 wt%), GP is fair in-between (1.79-3.03 mg)HC/g rock), kerogen types of (III-II/III), and HI within the range of 167–169 mg HC/g TOC of mainly terrestrial origin. These source rock intervals of 30.48 and 18.29 m thick are occupying only 17.52% of total Abu-Roash G thickness. Furthermore, the lower and upper source rock of Abu-Roash G alternative with the sandstone reservoirs represents the main essential pay zones in the studied basin of high MI (0.16-0.4), indicating in situ free HC generation.

In contrast, a late mature L-Kharita shows an end of oil generation and the start of gas-prone source rock at two main intervals of OM rich are 51.82 m in between 3372.61 and 3424.43 m depths and 39.62 m in between 3436.62 and 3476.24 m depths. These source rock intervals characterized by TOC of fair to good (1.02–1.72 wt%), GP of fair within the range of 0.94-3.09 mg HC/g rock, kerogen types (III), and low HI within the range of 82-145 mg HC/g TOC of mainly terrestrial origin. The gas-prone source rock intervals of L-Kharita comprise 60.97% (91.44 m) of entire thickness (149.96 m).

Organic-matter-rich interval (OMRI) versus organic matter poor interval (OMPI) diagram established by the authors (Figure 13) confirms that samples lay within these five OMRIs of effective source rock correspond to moderate and good potential, whereas samples showing a low potential or even nonsource of OMPI are those samples that do not belong to the five intervals in all presentative diagrams. So, our diagram will helpfully be a tool in any further interpretation to solve any geochemical disturbance data and to determine the actual thickness of effective source rocks in the studied basin.

The threshold of HC expulsion is recorded at the depth of 2,000 m, and ADSL of limit oil window is detected at a depth of 2,750 m by a different method. The BSB is considered a high-heat flow basin. Average calculated heat flow reach to be responsible for shallowing the HC expulsion depth in the basin to the recorded value, whereas in basins of either medium- or low-heat flow <75 mW/m<sup>2</sup>, it may reach deeper depths.

Burial history model postulates that Abu-Roash F and G source rocks are entering within the early oil generation since 56 Ma that confirms still an adequate quantity of hydrocarbon generation and expulsion for those source rocks. L-Kharita is now within the late oil stage where it generates most of its oil throughout its peak stage since 91 and 85 Ma.

**Acknowledgements:** The authors thank the EGPC for the permission provided to use geochemical data and welllog chart for the studied well to accomplish this study.

**Conflict of interest:** Authors state no conflict of interest.

#### References

- Sakran S, Shehata AA, Osman O, El-Sherbiny M. Superposed tectonic regimes in West Beni Suef Basin, Nile Valley, Egypt: implications to source rock maturation and hydrocarbon entrapment. J Afr Earth Sci. 2019;154:1-19.
- [2] Shehata AA, El Fawal FM, Ito M, Aboulmagd MA, Brooks HL. Senonian platform-to-slope evolution in the tectonicallyinfluenced Syrian Arc sedimentary belt: Beni Suef Basin, Egypt. J Afr Earth Sci. 2020;170:103-34.
- Makky AF, El Sayed MI, El-Ata ASA, Abd El-Gaied IM, Abdel-Fattah MI, Abd-Allah ZM. Source rock evaluation of some upper and lower cretaceous sequences, West Beni Suef concession, Western Desert, Egypt. Egypt J Pet. 2014;23(1):135-49.
- Shehata AA, El Fawal FM, Ito M, Aal MHA, Sarhan MA. Sequence stratigraphic evolution of the syn-rift Early Cretaceous sediments, West Beni Suef Basin, the Western Desert of Egypt with remarks on its hydrocarbon accumulations. Arab J Geosci. 2018;11(12):1-18.
- Bosworth W, El-Hawat AS, Helgeson DE, Burke K. Cyrenaican "shock absorber" and associated inversion strain shadow in the collision zone of northeast Africa. Geology. 2008;36(9):695-8.
- Abdel-Fattah MI, Pigott JD, Abd-Allah ZM. Integrative 1D-2D [6] basin modeling of the cretaceous Beni Suef Basin, Western Desert, Egypt. J Pet Sci Eng. 2017;153:297-313.
- Zahran H, Elyazid KA, Mohamad M. Beni Suef Basin the key for [7] exploration future success in Upper Egypt. Search Discovery Artic. 2011:10351:57-69.
- Abdel-Fattah MI, Alrefaee HA. Diacritical seismic signatures for complex geological structures: case studies from Shushan Basin (Egypt) and Arkoma Basin (USA). Int J Geophys. 2014;2014:1-11.
- [9] Hegazy A. Western desert oil and gas fields (A comprehensive overview). In: EGPC Conference Proceedings. Cairo: Egyptian General Petroleum Corporation; 1992. p. 4321.
- [10] Younes MA, Bek M. Alamein basin hydrocarbon potentials, northern Western Desert, Egypt. AAPG Annual Convention. Vol. 11. Salt Lake City: AAPG; 2003. p. 14.

- [11] Abdel-Fattah M, Gameel M, Awad S, Ismaila A. Seismic interpretation of the aptian Alamein dolomite in the razzak oil field, Western Desert, Egypt. Arab J Geosci. 2015;8(7):4669-84.
- [12] Hunt JM. Petroleum geochemistry and geology. 2nd edn. W. H. Freeman and Company; 1996. p. 743.
- [13] Walters C. The origin of petroleum. Practical advances in petroleum processing. Springer; 2006. p. 79-101. doi: 10.1007/978-0-387-25789-1 2.
- [14] Tissot BP, Welte DH. Petroleum formation and occurrence. 2nd edn. Berlin: Springer; 1984. p. 148–80
- [15] Waples DW. Maturity modelling: thermal indicators, hydrocarbon generation, and oilcracking. Am Assoc Pet Geolog Bull. 1994;60:285–306.
- [16] Said R. The geology of Egypt. Amsterdam, New York, USA: Elsevier; 1990. p. 197–214.
- [17] Guiraud R, Bosworth W, Thierry J, Delplanque A. Phanerozoic geological evolution of Northern and Central Africa: an overview. J Afr Earth Sci. 2005;43(1–3):83–143.
- [18] Salem E, Sehim A. Structural imaging of the East Beni Sueif Basin, north eastern Desert, Egypt. J Afr Earth Sci. 2017;136:109–18.
- [19] Moustafa AR. Mesozoic-Cenozoic basin evolution in the northern Western Desert of Egypt. Geol East Libya. 2008;3:29–46.
- [20] Meshref W. Tectonic framework. The Geology of Egypt; 1990. p. 113-55.
- [21] Bosworth W, Stockli DF, Helgeson DE. Integrated outcrop, 3D seismic, and geochronologic interpretation of Red Sea dikerelated deformation in the Western Desert, Egypt-The role of the 23 Ma Cairo "mini-plume". J Afr Earth Sci. 2015;109:107-19.
- [22] Dolson JC, Shann MV, Hammouda H, Rashed R, Matbouly S. The petroleum potential of Egypt. AAPG Bull. 1999;83(12):17-27.
- [23] Sestini G. Tectonic and sedimentary history of the NE African margin (Egypt-Libya). Geol Soc (London Spec Publ). 1984;17(1):161-75.
- [24] EGPC Egyptian General Petroleum Corporation. Western
  Desert, oil and gas fields, a comprehensive overview. 11th EGPC
  Exploration and Production Conference Cairo; 1992. p. 1–431.
- [25] El Batal A, Abdelwhab O, Clerk C, Abdo M. Effect of lacustrine petroleum source rock on the distribution of the recoverable oil accumulations, Beni-Suef basin, Western Desert, Egypt. In: 13th Mediterranean Offshore Conference and Exhibition (MOC). Alex, Egypt: AAPG; 2016. p. 19–21.
- [26] Espitalie J, Deroo G, Marquis F. Rock-eval pyrolysis and its application. 1st edn. Paris: Inst. Fr. Preprint; 1985. p. 72.
- [27] Peters KE, Cassa MR. Applied source rock geochemistry. In: Magoonand LB, Dow WG, editors. The petroleum system from source to trap. AAPG; 1994. p. 93–120.

- [28] Espitalie JM, Laporte JL, Madec M, Marquis F, Laplot P, Paulet J, et al. Rapid method for source rock characterization, and for determination of their petroleum potential and degree of evolution. Rev de l'Inst Francais du Petrole et Ann des Comb Liq. 1997;32:23–4.
- [29] Jarvie DM, Morelos A, Han Z. Detection of pay zones and pay quality. Gulf of Mexico: application of geochemical techniques. Gulf Coast Assoc Geol Soc Trans. 2001;51:151-60.
- [30] Gürgey K, Bati Z. Palynological and petroleum geochemical assessment of the Lower Oligocene Mezardere Formation, Thrace Basin, NW Turkey. Turkish J Earth Sci. 2018;27:349–83.
- [31] Pang X, Jia C, Zhang K, Li M, Wang Y, Peng J, et al. The depth limit for the formation and occurrence of fossil fuel resources. Earth Syst Sci Data Discuss. 2019;72:1–26. doi: 10.5194/essd-2019-72.
- [32] Smith JT. Petroleum system logic as an exploration tool in frontier setting. In: Magoon LP, Dow WG, editors. The petroleum system from source to trap. Vol. 60. AAPG Memoir; 1994. p. 25–49.
- [33] Ghori KAR, Haines PW. Paleozoic petroleum systems of the Canning Basin, Western Australia: a review. Search Discovery Artic. 2007;10120:5–8.
- [34] Vandenbroucke M, Largeau C. Kerogen origin, evolution and structure. Org Geochem. 2007;38:719–833.
- [35] Langford FF, Balanc-Valleron MM. Interpreting Rock-Eval pyrolysis data using graphs of pyrolizable hydrocarbons vs. total organic carbon. AAPG Bull. 1990;74:799–804.
- [36] Delvaux D, Martin H, Leplat P, Paulet J. Geochemical characterization of sedimentary organic matter by means of pyrolysis kinetic. In: Durand B, Behar F, editors. Advances in organic geochemistry 1989. Vol 16. Pergamon, Oxford: Organic Geochemistry; 1990. p. 175–87.
- [37] Bacon CA, Calver CR, Boreham CJ, Leaman DE, Morrison KC, Revill AT, et al. The petroleum potential of onshore Tasmania: a review. Mineral resources Tasmania. Geol Surv Bull. 2000;71:1–93.
- [38] Koeverdon JHV, Karlsen DA. Backer-Owe K. Carboniferous non-marine source rocks from Spitsbergen and Bajornoya: comparison with western Arctic. J Pet Geol. 2011;34(1):53-66.
- [39] Jiang F, Pang X, Guo J, Zhou X, Zhou X, Liu D, et al. Identification and hydrocarbon expulsion history simulation of the effective source rocks in the Dongying formation, Paleogene, Bohai Sea area, eastern China. Rev Mexicana de Cienc Geológicas. 2013;30(2):355-70.
- [40] Sweeney JJ, Burnham AK. Evaluation of a simple model of vitrinite reflectance based on chemical kinetics. Am Assoc Pet Geol Bull. 1990;74:1559–70.